crystals

MDPI

Article

High-Peak-Power Passively Q-Switched Laser at 589 nm with Intracavity Stimulated Raman Scattering

Jian-Cheng Chen [1], Yu-Wen Ho [1], Yueh-Chi Tu [1], Hsing-Chih Liang [2] and Yung-Fu Chen [1,*]

[1] Department of Electrophysics, National Yang Ming Chiao Tung University, Hsinchu 30010, Taiwan
[2] Institute of Optoelectronic Science, National Taiwan Ocean University, Keelung 20224, Taiwan
* Correspondence: yfchen@nycu.edu.tw

Abstract: A novel scheme was developed for a diode-pumped passively Q-switched Nd:YVO_4/KGW Raman laser at 589 nm with a diode-to-orange conversion efficiency reaching 11.4%. The compact near-concentric cavity was designed to achieve the criterion of good passive Q-switching and to contain a coupled resonator for intracavity stimulated Raman scattering (SRS) and second harmonic generation (SHG). The dependence of the output performance on the initial transmission of the saturable absorber was explored in detail. Furthermore, the output performance was studied by considering the influence of the pump-to-mode size ratio. By using an initial transmission of 50%, the highest pulse energy and peak power were 110 μJ and 118 kW, respectively, at a pump duration of 40 μs and a pump frequency of 10 kHz.

Keywords: stimulated Raman scattering; passively Q-switched laser; KGW crystal

Citation: Chen, J.-C.; Ho, Y.-W.; Tu, Y.-C.; Liang, H.-C.; Chen, Y.-F. High-Peak-Power Passively Q-Switched Laser at 589 nm with Intracavity Stimulated Raman Scattering. *Crystals* **2023**, *13*, 334. https://doi.org/10.3390/cryst13020334

Academic Editor: Sergei Smetanin

Received: 30 January 2023
Revised: 12 February 2023
Accepted: 14 February 2023
Published: 16 February 2023

1. Introduction

High-peak-power pulsed lasers at 550–600 nm are very useful in applications such as medical skin treatments [1], biological detection [2], optical-resolution photoacoustic microscopy [3], and stimulated emission depletion microscopy [4]. Light sources at 589 nm are particularly important for applications such as atmospheric lidar measurement [5,6], adaptive optics [7], and sodium guide stars [8,9]. The technologies for developing orange light sources at 589 nm involve dye lasers, diode-pumped solid-state lasers, optically pumped semiconductor lasers, and fiber lasers [10]. The combination of intracavity stimulated Raman scattering (SRS) and second harmonic generation (SHG) in a diode-pumped solid-state Q-switched laser is nowadays the most efficient method for achieving a high-peak-power output [11–18]. In addition to Q-switched operation, the concept of using the intracavity Raman and SHG conversion in a diode-pumped neodymium laser to obtain yellow-orange radiation has been efficiently realized in continuous-wave and quasi-continuous-wave regimes [19–27].

Compared with active Q-switching, the benefits of passive Q-switching consist in its simplicity, compactness, and light weight [28–31]. However, due to the fluctuations of the pump and emission, passively diode-pumped Q-switched lasers usually suffer from a timing jitter in the output pulses [32]. Nevertheless, the timing jitter can be significantly improved using a pulse pumping scheme based on short pump duration and a high pump power [33]. In addition to reducing the timing jitter, pulse pumping can also significantly decrease the thermal lensing effect. So far, the diode-to-orange conversion efficiency achieved by passive Q-switching is between 1.2 and 7.3%, never exceeding 10% [34,35].

In this work, we originally exploited a near-concentric resonator to achieve an efficient passively Q-switched Nd:YVO_4 Raman laser at 589 nm with potassium gadolinium tungstate (KGW) as an intracavity Raman gain medium at the shift of 901 cm^{-1}. The near-concentric resonator was used to provide a beam focusing on the saturable absorber to accomplish good passive Q-switching and to include a coupled cavity for performing

the SRS and SHG. Three different saturable absorbers were utilized to thoroughly explore the dependence of the output performance on the initial transmission. Furthermore, we also investigated in detail the influence of the pump-to-mode size ratio on the output characterization. By using the pulse pumping scheme at a pump frequency of 10 kHz, the highest pulse energy and peak power were 110 μJ and 70 kW, respectively. The optimal diode-to-orange conversion efficiency reached 11.4%, which is, to the best of our knowledge, the highest efficiency ever reported for a diode-end-pumped passively Q-switched Raman laser.

2. Cavity Design and Experimental Setup

Figure 1 shows the experimental configuration for generating the orange laser at 589 nm in a passively Q-switched Nd:YVO_4/KGW Raman laser with intracavity SRS and SHG. We designed the resonator to be a concave-concave symmetrical cavity for the fundamental wave and to include a coupled plano-concave cavity for the Raman Stokes wave. For the pump source, we exploited a fiber-coupled semiconductor laser at 808 nm with a maximum output power of 40 W. The coupling fiber had the specifications of a 100 μm core radius and a 0.22 numerical aperture. For the laser gain medium, we utilized an *a*-cut Nd:YVO_4 crystal with a Nd^{3+} concentration of 0.2 at.% and dimensions of $3 \times 3 \times 20$ mm^3. Both end facets of the gain medium had an anti-reflective (AR) coating in the spectral region of 1060–1180 nm (reflectance < 0.2%). The radius of curvature of the rear concave mirror was 85 mm. On the facet toward the pump side, the rear mirror was coated to be AR at 808 nm (reflectance < 0.2%). On the concave facet, the rear mirror was coated to be highly reflective (HR) in the spectral range of 1000–1200 nm (reflectance > 99.9%) and highly transmissive (HT) at 808 nm (transmittance > 95%). For the saturable absorber, we employed three different Cr^{4+}:YAG crystals with initial transmissions of T_o = 50%, 60%, and 70% to investigate the output performance. All Cr^{4+}:YAG crystals had the same dimensions of $3 \times 3 \times 2$ mm^3. Both end facets of the Cr^{4+}:YAG crystal were coated to be AR in the spectral region of 1060–1180 nm (reflectance < 0.2%). For the Raman gain medium, we used a N_p-cut KGW crystal with dimensions of $3 \times 3 \times 20$ mm^3. In the experiment, we arranged the polarization of the fundamental wave to be along the N_m axis of the KGW crystal in order to favor the Raman shift of 901 cm^{-1}. On the facet toward the Nd:YVO_4 crystal, the KGW crystal had a HR coating at 1178 nm (reflectance > 99.9%) and a HT coating at 1064 nm (transmittance > 99%). On the other facet, the KGW crystal had a HT coating at 1064 nm and 1178 nm (transmittance > 99%) and a HR coating at 589 nm (reflectance > 99%) to reflect the orange light that was generated in the backward direction. We exploited indium foils to wrap the Nd:YVO_4, Cr^{4+}:YAG, and KGW crystals and then mounted these crystals in the copper holders with active cooling at 20 °C. For the nonlinear crystal, we used an LBO crystal with a length of 8 mm and cut angles of $\theta = 90^\circ$ and $\phi = 3.9^\circ$ for the critical phase matching to produce the orange laser at 589 nm via the intracavity SHG of the Stokes wave at 1178 nm. Both end facets of the LBO crystal had AR coatings at 1064, 1178, and 589 nm. We utilized a thermoelectric cooler to precisely control the temperature of the LBO crystal in order to achieve the optimal phase matching. A concave mirror with a radius of curvature of 85 mm was used as the output coupler. The concave side of the output coupler was coated to be HR at 1060–1180 nm (reflectance > 99.9%) and HT at 589 nm (transmittance > 95%). The other side was coated to be AR at 589 nm (reflectance < 0.2%). The Nd:YVO_4 crystal was positioned very close to the rear mirror with a separation of approximately 1.0 mm. The Cr^{4+}:YAG crystal was placed in the center of the cavity, i.e., the location of the beam waist. The crystals of Cr^{4+}:YAG, KGW, and LBO were positioned very close to each other with separations of approximately 1.0 mm. The geometric length for the fundamental wave cavity was approximately 188 mm to form a near-concentric configuration. Three different pairs of coupling lenses were employed to focus the pump light into the laser crystal, resulting in three different pump radii of ω_p = 210, 320, and 430 μm for investigating the output performance.

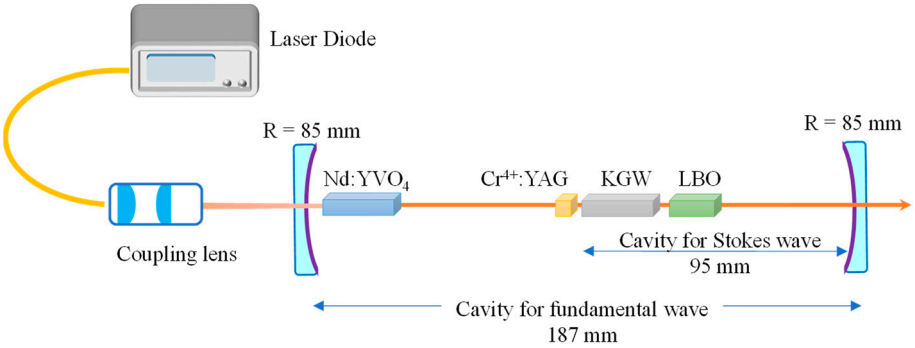

Figure 1. Experimental configuration for generating the orange laser at 589 nm in a passively Q-switched Nd:YVO_4/KGW Raman laser with intracavity SRS and SHG.

Let L_{cav} be the geometric length for the fundamental wave cavity. The optical length L^*_{cav} for the laser cavity is then given by:

$$L^*_{cav} = L_{cav} - \sum_{j=1}^{4} \left(1 - \frac{1}{n_j}\right) \ell_j \tag{1}$$

where ℓ_1, ℓ_2, ℓ_3, and ℓ_4 are the lengths of the Nd:YVO_4, Cr^{4+}:YAG, KGW, and LBO crystals, respectively, and n_1, n_2, n_3, and n_4 are the refractive indices of their counterparts. According to the experimental setup with L_{cav} = 188 mm, Equation (1) could be used to find that the value of L^*_{cav} was approximately 160 mm. Note that the refractive indices used in the calculation were the data without considering the influences of the doping concentration and temperature. For the present concave-concave symmetric resonator, the cavity mode radius on the rear mirror is given by:

$$\omega_1 = \left[\frac{\lambda R}{\pi}\sqrt{\frac{L^*_{cav}}{(2R - L^*_{cav})}}\right]^{1/2} \tag{2}$$

where λ is the wavelength of the fundamental wave, and R is the radius of curvature for both concave mirrors of the laser cavity. The cavity mode radius at the beam waist is given by:

$$\omega_o = \left[\frac{\lambda}{2\pi}\sqrt{L^*_{cav}(2R - L^*_{cav})}\right]^{1/2} \tag{3}$$

Since the Nd:YVO_4 crystal was positioned very close to the rear mirror, the cavity mode radius in the gain medium could be approximated as $\omega_c \approx \omega_1$. Substituting L^*_{cav} = 160 mm and R = 85 mm into Equation (2), the value of ω_c could be found to be around 340 µm. On the other hand, since the Cr^{4+}:YAG crystal was placed at the location of the beam waist, the mode radius in the saturable absorber could be approximated as $\omega_s \approx \omega_o$. Substituting L^*_{cav} = 160 mm and R = 85 mm into Equation (3), the value of ω_s could be found to be around 80 µm. Consequently, the mode area ratio $A/A_s = \omega_c^2/\omega_s^2$ could be found to reach 16, where A and A_s are the mode areas in laser crystal and saturable absorber, respectively.

From the rate equations for a four-level passively Q-switched operation [36], the performance of the passive Q-switching could be shown to be mainly determined by the following parameter:

$$\alpha = A\sigma_{gs}/(\gamma A_s \sigma) \tag{4}$$

where σ is the stimulated emission cross-section of the gain medium, γ is the inversion reduction factor, and σ_{gs} is the absorption cross-sections of the ground state of the saturable absorber. A theoretical analysis was performed to verify that the higher the parameter α, the better the possible output performance [36]. Nevertheless, when the value of α was greater than 5.0, there was not much room for boosting the efficiency of the passive

Q-switching. By using the following parameters for the present experiment, $A/A_s = 18$, $\sigma = 15.6 \times 10^{-19}$ cm^2, $\sigma_{gs} = 8.7 \times 10^{-19}$ cm^2, and $\gamma = 1$, we could calculate the value of the parameter α to be nearly 10.0. In other words, the present cavity design could lead to high-quality passive Q-switching.

The coupled cavity for the SRS process was formed by the coated KGW crystal and the output coupler. The geometric length of the coupled cavity for the Stokes wave was approximately $L_{SRS} = 95$ mm. The optical length for the SRS cavity is given by:

$$L^*_{SRS} = L_{SRS} - \left(1 - \frac{1}{n_3}\right)\ell_3 - \left(1 - \frac{1}{n_4}\right)\ell_4 \quad (5)$$

Accordingly, the optical length L^*_{SRS} was found to be approximately 80 mm. To be brief, the SRS cavity had a near-hemispherical configuration. With $L^*_{cav} = 160$ mm, the optical length for the SRS cavity was confirmed to be close to half of that for the fundamental wave. The cavity mode radius for the Stokes wave on the facet with the dichroic coating of the KGW crystal is given by:

$$\omega_R = \left[\frac{\lambda_R}{\pi}\sqrt{L^*_{SRS}(R - L^*_{SRS})}\right]^{1/2} \quad (6)$$

where λ_R is the wavelength of the Stokes wave. Since $L^*_{cav} = 2L^*_{SRS}$, we could confirm the mode matching between the fundamental and Raman Stokes waves from Equations (3) and (6).

3. Experimental Results and Discussion

The polarization states for the fundamental and Raman Stokes waves were self-controlled to be linearly polarized due to the gain anisotropies in the *a*-cut Nd:YVO4 and N_p-cut KGW crystals, respectively. The pump power of the laser diode was electronically operated at a pump duration of 40 μs with a pump frequency of 10 kHz. Figure 2 shows the experimental results for the pump threshold energy at 808 nm versus the initial transmission T_o of the saturable absorber under three different pump-to-mode size ratios ω_p/ω_c for the output pulse rate to reach the pump rate of 10 kHz. The pump threshold energy was found to increase with a decrease in the initial transmission T_o, because a lower initial transmission T_o led to a larger stored energy in the laser crystal. On the other hand, the pump threshold energy increased with an increase in the ratio ω_p/ω_c. The increasing trend was confirmed to be proportional to the effective mode area $\pi(\omega_p^2 + \omega_c^2)$, consistent with the theoretical analysis [36]. For the case of $\omega_p/\omega_c = 1.34$, the pump threshold energy was seen to increase from 0.58 to 0.94 mJ as the initial transmission T_o lowered from 70% to 50%.

Although the pump threshold energy increased with a decrease in the initial transmission T_o and an increase in the ratio ω_p/ω_c, the output pulse energy at 589 nm was found to increase with a similar tendency. Figure 3 depicts the experimental results for the output pulse energy at 589 nm versus the initial transmission T_o of the saturable absorber for three different pump-to-mode size ratios ω_p/ω_c. For the case of $\omega_p/\omega_c = 1.34$, the output pulse energy at 589 nm increased from 0.06 to 0.11 mJ as the initial transmission T_o lowered from 70% to 50%. On the other hand, the output pulse energy increased from 0.068 to 0.11 mJ as the ratio ω_p/ω_c increased from 0.66 to 1.34 for the case of $T_o = 50\%$. On the whole, the diode-to-orange conversion efficiencies for three different ratios ω_p/ω_c and three initial transmissions T_o were all higher than 10%. The highest efficiency reached 11.4%, obtained with $\omega_p/\omega_c = 1.34$ and $T_o = 50\%$. The conversion efficiency from 808 nm to 1064 nm was approximately 50~60%. Therefore, we roughly estimated that both conversion efficiencies from 1064 nm to 1178 nm and from 1178 nm to 589 nm were approximately 20~30%.

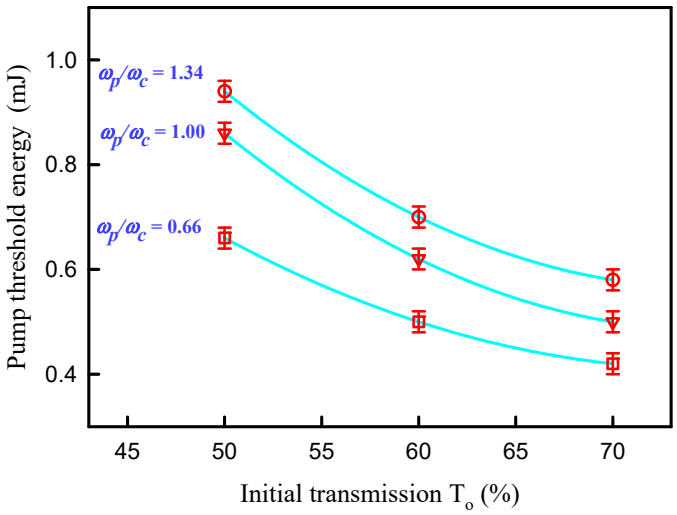

Figure 2. Experimental results for the pump threshold energy at 808 nm versus the initial transmission T_o of the saturable absorber under three different pump-to-mode size ratios ω_p/ω_c for the output pulse rate to reach the pump rate of 10 kHz.

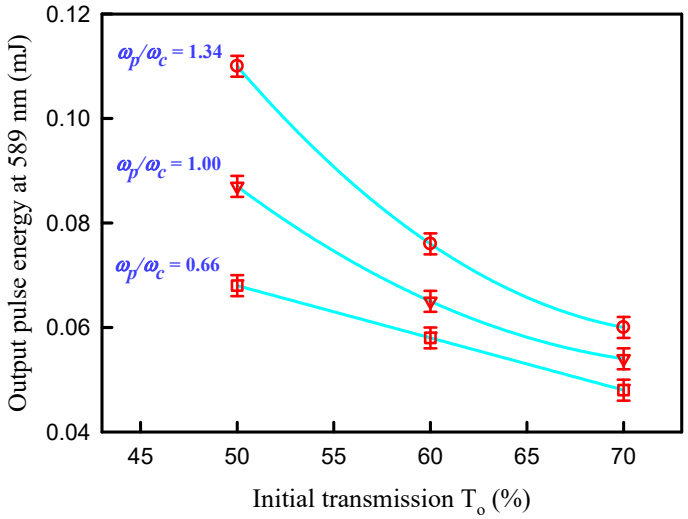

Figure 3. Experimental results for the output pulse energy at 589 nm versus the initial transmission T_o of the saturable absorber for three different pump-to-mode size ratios ω_p/ω_c.

Figure 4 shows the experimental results for the average output power at 589 nm versus the average input power at 808 nm for three different initial transmissions T_o of the saturable absorbers when ω_p/ω_c = 1.34. It was obvious that there were steps for the different passive Q-switchers. The final step for each saturable absorber shown in Figure 4 represented an output pulse rate equal to the pump rate of 10 kHz. The steps before the final step revealed the output pulse rate to be a fraction of the pump rate. Nevertheless, it is easier to estimate the real efficiency of the laser from Figure 4.

Figure 5 shows the experimental results for the pulse width at 589 nm versus the initial transmission T_o of the saturable absorber for three different pump-to-mode size ratios ω_p/ω_c. The pulse width was seen to shorten with a decrease in the initial transmission T_o for a given ratio ω_p/ω_c. The overall pulse width was seen to be as short as 0.91 to 2.1 ns for the three different ratios ω_p/ω_c and three initial transmissions T_o. The pulse shortening effect can be clearly seen due to the intracavity stimulated Raman scattering in passive Q-switched lasers [37–40]. As shown in Figure 3, the enlargement in the pump-to-mode size ratio ω_p/ω_c could lead to an increase in the output pulse energy. Similarly, the pulse width could be narrowed by increasing the pump-to-mode size ratio. Using ω_p/ω_c = 1.34

for the saturable absorber with T_o = 50%, the pulse width was experimentally found to be as short as 0.91 ns.

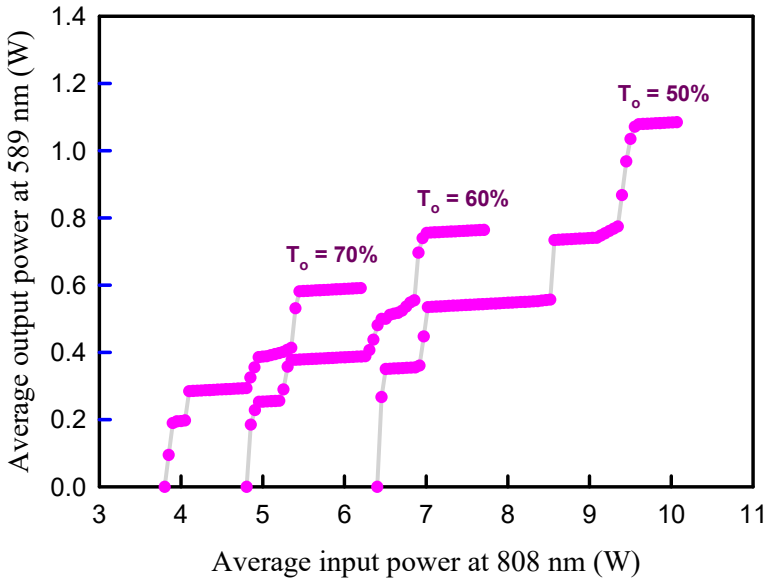

Figure 4. Experimental results for the average output power at 589 nm versus the average input power at 808 nm for three different initial transmissions T_o of the saturable absorbers when ω_p/ω_c = 1.34.

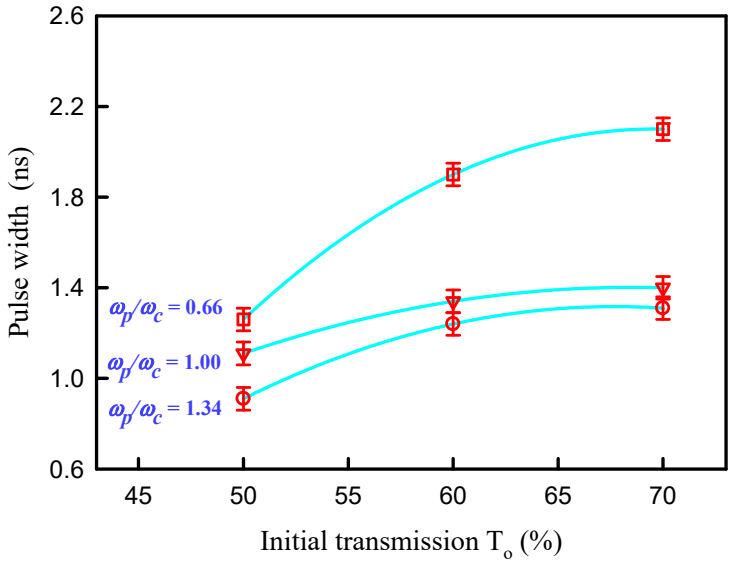

Figure 5. Experimental results for the pulse width at 589 nm versus the initial transmission T_o of the saturable absorber for three different pump-to-mode size ratios ω_p/ω_c.

The peak-to-peak fluctuation in the pulse train could be optimized to be approximately ±5.5%. The typical pulse train and temporal profile for the orange output at 589 nm obtained with ω_p/ω_c = 1.34 and T_o = 50% are shown in Figure 6. The temporal profile revealed the output pulse to be a pure single pulse without a satellite pulse. Furthermore, no significant modulation was observed in the temporal profile of the output pulse. Accordingly, the number of longitudinal modes seemed to be close to the number of single modes. The selection of the longitudinal modes may be attributed to the shortness of the coupled cavity and the several etalon effects caused by the small separations among the Cr^{4+}:YAG, KGW, and LBO crystals. On the other hand, the spatial quality of the output beam was also examined. The beam quality factor M^2 was measured by the traveling knife-edge method. The overall beam quality was found to be within 1.5~2.0 at an output rate of up to 10 kHz for the three different saturable absorbers.

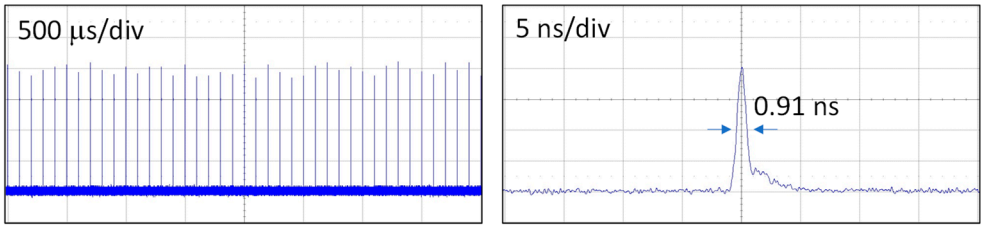

Figure 6. Typical pulse train and temporal profile for the orange output at 589 nm obtained with ω_p/ω_c = 1.34 and T_o = 50%.

The output peak power was evaluated using the experimental data of the output pulse energy and pulse width. Figure 7 shows the calculated results for the output peak power at 589 nm versus the initial transmission T_o of the saturable absorber for three different pump-to-mode size ratios ω_p/ω_c. The output peak power was seen to increase with a decrease in the initial transmission T_o. Similar to the output energy, the output peak power increased with an increase in the pump-to-mode size ratio ω_p/ω_c. Using ω_p/ω_c = 1.34, the output peak power obtained with T_o = 50% was found to reach 118 kW. To the best of our knowledge, this is the highest peak power obtained in a diode-end-pumped passively Q-switched solid-state Raman laser at 589 nm. We used an optical spectrum analyzer (Advantest Q8381A) with a resolution of 0.1 nm to measure the optical spectrum of the output beam. Figure 8 shows the typical optical spectrum observed for the output beam. The lasing wavelength can be seen to be around 589 nm.

Finally, it is worthwhile to discuss the thermal effect in the present work. The thermal properties of KGW crystals have been confirmed to be strongly anisotropic [41]. As shown in Figure 1 for the resonator configuration, the coupled cavity for the intracavity SRS was formed by a coated KGW crystal and an output coupler. Due to the anisotropy of the thermal properties of KGW crystals, the output coupler for the SRS cavity needed to be a concave mirror to achieve cavity stability. When the output coupler was replaced by a flat mirror, the laser output at 589 nm was experimentally found to exhibit significant fluctuation and a low conversion efficiency. The thermal effects for the comparison between self-Raman Nd: YVO_4 lasers and Nd:YVO_4/KGW Raman lasers at lime and orange wavelengths can be found in ref. [24].

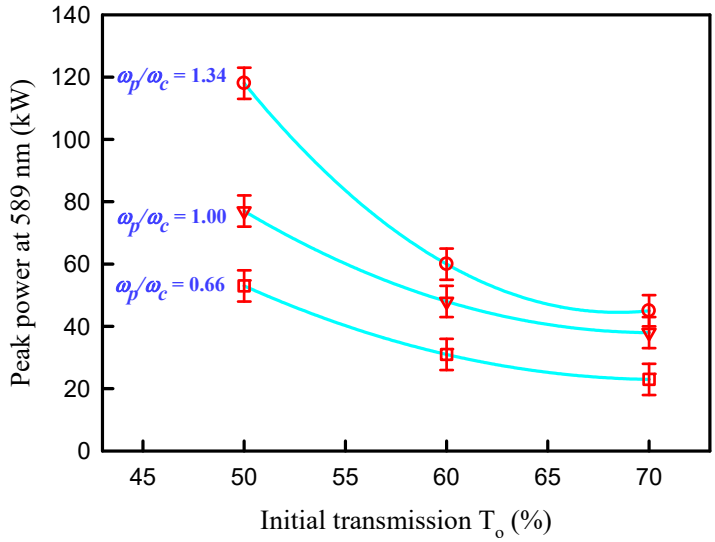

Figure 7. Calculated results for the output peak power at 589 nm versus the initial transmission T_o of the saturable absorber for three different pump-to-mode size ratios ω_p/ω_c.

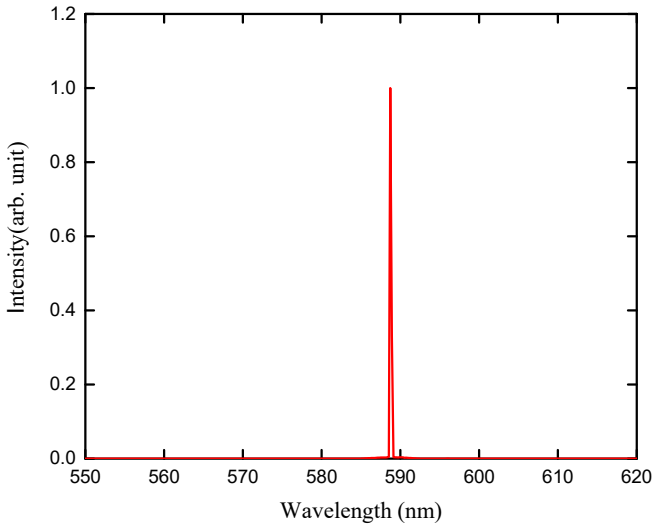

Figure 8. Typical optical spectrum observed for the output beam.

4. Conclusions

In summary, we developed a near-concentric resonator for a passively Q-switched Nd:YVO_4 laser at 589 nm with a Raman KGW crystal to achieve a diode-to-orange conversion efficiency of up to 11.4%. We designed a compact near-concentric cavity to focus on the saturable absorber in order to satisfy the criterion of good passive Q-switching and to include a coupled resonator for SRS together with SHG. We also systematically explored the influence of the pump size on the output performance. By using a pump duration of 40 μs and a pump frequency of 10 kHz, the optimal pulse energy and peak power generated with T_o = 50% reached 110 μJ and 118 kW, respectively.

Author Contributions: Conceptualization, J.-C.C. and Y.-F.C.; validation, Y.-W.H. and H.-C.L.; formal analysis, J.-C.C. and H.-C.L.; resources, Y.-W.H. and Y.-C.T.; writing—original draft preparation, Y.-F.C.; writing—review and editing, J.-C.C., Y.-C.T. and Y.-F.C.; supervision, Y.-F.C. All authors have read and agreed to the published version of the manuscript.

Funding: This work was supported by the Ministry of Science and Technology of Taiwan (contract number 109-2112-M-009-015-MY3).

Institutional Review Board Statement: Not applicable.

Informed Consent Statement: Not applicable.

Data Availability Statement: All of the data reported in the paper are presented in the main text. Any other data will be provided on request.

Conflicts of Interest: The authors declare no conflict of interest.

References

1. Cho, S.; Choi, Y.J.; Kang, J.-S. Treatment of epidermal pigmented lesions with 578 nm yellow laser. *Med. Lasers* **2015**, *4*, 35–38. [CrossRef]
2. Long, H.; Liu, M.; Hu, Q.; Li, X. 577 nm subthreshold micropulse laser treatment for acute central serous chorioretinopathy: A comparative study. *BMC Ophthalmol.* **2022**, *22*, 105. [CrossRef] [PubMed]
3. Maslov, K.; Zhang, H.F.; Hu, S.; Wang, L.V. Optical-resolution photoacoustic microscopy for in vivo imaging of single capillaries. *Opt. Lett.* **2008**, *33*, 929. [CrossRef] [PubMed]
4. Runcorn, T.H.; Görlitz, F.G.; Murray, R.T.; Kelleher, E.J.R. Visible Raman-shifted Fiber Lasers for Biophotonic Applications. *IEEE J. Sel. Top. Quant. Electron.* **2018**, *24*, 1400208. [CrossRef]
5. Ernstberger, B.; Enderlein, M.; Friedenauer, A.; Schwerdt, R.; Wei, D.; Karpov, V.; Leisching, P.; Clements, W.R.L.; Kaenders, W.G. Robust remote-pumping sodium laser for advanced LIDAR and guide star applications. *SPIE Remote Sens.* **2015**, *9641*, 96410F.
6. Jones, K.J. Progress in Na laser guide star adaptive optics and lessons learned. *Proc. SPIE* **2016**, *9950*, 995011.
7. Huo, X.; Qi, Y.; Zhang, Y.; Chen, B.; Bai, Z.; Ding, J.; Wang, Y.; Lu, Z. Research development of 589 nm laser for sodium laser guide stars. *Opt. Lasers Eng.* **2020**, *134*, 106207. [CrossRef]

8. Bian, Q.; Bo, Y.; Zuo, J.; Li, M.; Dong, R.; Deng, K.; Zhang, D.; He, L.; Zong, Q.; Cui, D.; et al. Investigation of return photons from sodium laser beacon excited by a 40-watt facility-class pulsed laser for adaptive optical telescope applications. *Sci. Rep.* **2018**, *8*, 9222. [CrossRef]
9. Yang, X.; Zhang, L.; Cui, S.; Fan, T.; Dong, J.; Feng, Y. Sodium guide star laser pulsed at Larmor frequency. *Opt. Lett.* **2017**, *42*, 4351–4354. [CrossRef]
10. Zhang, L.; Duan, Y.; Sun, Y.; Chen, Y.; Li, Z.; Zhu, H.; Zhang, G.; Tang, D. Passively Q-switched multiple visible wavelengths switchable YVO_4 Raman laser. *J. Lumin.* **2020**, *228*, 117650. [CrossRef]
11. Zhu, H.; Duan, Y.; Zhang, G.; Huang, C.; Wei, Y.; Shen, H.; Zheng, Y.; Huang, L.; Chen, Z. Efficient second harmonic generation of double-end diffusion-bonded Nd:YVO_4 self-Raman laser producing 7.9 W yellow light. *Opt. Express* **2009**, *17*, 21544–21550. [CrossRef] [PubMed]
12. Duan, Y.M.; Zhu, H.Y.; Huang, C.H.; Zhang, G.; Wei, Y. Potential sodium D_2 resonance radiation generated by intra-cavity SHG of a *c*-cut Nd:YVO_4 self-Raman laser. *Opt. Express* **2011**, *19*, 6333–6338. [CrossRef] [PubMed]
13. Shen, H.; Wang, Q.; Zhang, X.; Chen, X.; Cong, Z.; Bai, F.; Gao, L.; Lan, W. Intracavity frequency-doubled Nd:YAG/$KLu(WO_4)_2$ Raman laser at 589 nm: A potential source for sodium D_2 resonance radiation. *Opt. Laser Technol.* **2013**, *45*, 142–146. [CrossRef]
14. Liu, Y.; Liu, Z.; Cong, Z.; Men, J.; Rao, H.; Xia, J.; Zhang, S.; Zhang, H. Quasi-continuous-wave 589-nm radiation based on intracavity frequency-doubled Nd:GGG/$BaWO_4$ Raman laser. *Opt. Laser Technol.* **2016**, *81*, 184–188. [CrossRef]
15. Omatsu, T.; Okida, M.; Minassian, A.; Damzen, M. High repetition rate Q-switching performance in transversely diode-pumped Nd doped mixed gadolinium yttrium vanadate bounce laser. *Opt. Express* **2006**, *14*, 2727–2734. [CrossRef]
16. He, F.; Huang, L.; Gong, M.; Liu, Q.; Yan, X. Stable acousto-optics Q-switched Nd:YVO_4 laser at 500 kHz. *Laser Phys. Lett.* **2007**, *4*, 511–514. [CrossRef]
17. Chen, Y.F.; Chen, K.Y.; Liu, Y.C.; Chen, C.M.; Tsou, C.H.; Liang, H.C. Criterion for optimizing high-power acousto-optically Q-switched self-Raman yellow lasers with repetition rates up to 500 kHz. *Opt. Lett.* **2020**, *45*, 1922–1925. [CrossRef]
18. Wang, B. Low threshold, actively Q-switched Nd^{3+}: YVO_4 self-Raman laser and frequency doubled 588 nm yellow laser. *Opt. Commun.* **2007**, *271*, 555–558. [CrossRef]
19. Peter, D.; Pask, H.M.; Piper, J.A. All-solid-state 704 mW continuous-wave yellow source based on an intracavity, frequency-doubled crystalline Raman laser. *Opt. Lett.* **2007**, *32*, 1114–1116.
20. Piper, J.A.; Pask, H.M. Crystalline Raman lasers. *IEEE J. Sel. Top. Quant. Electron.* **2007**, *13*, 692–704. [CrossRef]
21. Lee, A.J.; Spence, D.J.; Piper, J.A.; Pask, H.M. A wavelength-versatile, continuous-wave, self-Raman solid-state laser operating in the visible. *Opt. Express* **2010**, *18*, 20013–20018. [CrossRef] [PubMed]
22. Lee, A.J.; Pask, H.M.; Piper, J.A.; Zhang, H.; Wang, J. An intracavity, frequency-doubled $BaWO_4$ Raman laser generating multi-watt continuous-wave, yellow emission. *Opt. Express* **2010**, *18*, 5984–5992. [CrossRef]
23. Chen, Y.F.; Pan, Y.Y.; Liu, Y.C.; Cheng, H.P.; Tsou, C.H.; Liang, H.C. Efficient high-power continuous-wave lasers at green-lime-yellow wavelengths by using a Nd:YVO_4 self-Raman crystal. *Opt. Express* **2019**, *27*, 2029–2035. [CrossRef] [PubMed]
24. Lee, C.-C.; Huang, C.-Y.; Huang, H.-Y.; Chen, C.-M.; Tsou, C.-H. Comparison between Self-Raman Nd:YVO_4 Lasers and $NdYVO_4$/KGW Raman Lasers at Lime and Orange Wavelengths. *Appl. Sci.* **2021**, *11*, 11068. [CrossRef]
25. Chen, Y.F.; Huang, H.Y.; Lee, C.C.; Hsiao, J.Q.; Tsou, C.H.; Liang, H.C. High-power diode-pumped Nd:$GdVO_4$/KGW Raman laser at 578 nm. *Opt. Lett.* **2020**, *45*, 5562–5565. [CrossRef]
26. Chen, Y.F.; Chen, C.M.; Lee, C.C.; Huang, H.Y.; Li, D.; Hsiao, J.Q.; Tsou, C.H.; Liang, H.C. Efficient solid-state Raman yellow laser at 579.5 nm. *Opt. Lett.* **2020**, *45*, 5612–5615. [CrossRef]
27. Chen, Y.F.; Li, D.; Lee, Y.M.; Lee, C.C.; Huang, H.Y.; Tsou, C.H.; Liang, H.C. Highly efficient solid-state Raman yellow-orange lasers created by enhancing the cavity reflectivity. *Opt. Lett.* **2021**, *46*, 797–800. [CrossRef] [PubMed]
28. Zayhowski, J.J. Passively Q-switched microchip lasers. In *Solid-State Lasers and Applications*; CRC Press: London, UK, 2007; pp. 1–75.
29. Degnan, J.J. Optimization of passively Q-switched lasers. *IEEE J. Quant. Electron.* **1995**, *31*, 1890–1901. [CrossRef]
30. Zhang, X.; Zhao, S.; Wang, Q.; Zhang, Q.; Sun, L.; Zhang, S. Optimization of Cr^4+-doped saturable-absorber Q-switched lasers. *IEEE J. Quant. Electron.* **1997**, *33*, 2286–2294. [CrossRef]
31. Pavel, N.; Tsunekane, M.; Taira, T. Composite, all-ceramics, high-peak power Nd:YAG/Cr^{4+}:YAG monolithic micro-laser with multiple-beam output for engine ignition. *Opt. Express* **2011**, *19*, 9378–9384. [CrossRef]
32. Negri, J.R.; Pirzio, F.; Agnesi, A. Jitter investigation of narrow-bandwidth passively Q-switched Nd:YAG unidirectional ring laser. *Opt. Lett.* **2019**, *44*, 3094–3097. [CrossRef] [PubMed]
33. Chen, Y.F.; Chien, P.Y.; Lee, C.C.; Huang, K.F.; Liang, H.C. Timing jitter reduction of passively Q-switched solid-state lasers by coupling resonance between pumping and firing rates. *Opt. Lett.* **2020**, *45*, 2902–2905. [CrossRef] [PubMed]
34. Chen, M.; Dai, S.; Yin, H.; Zhu, S.; Li, Z.; Chen, Z. Passively Q-switched yellow laser at 589 nm by intracavity frequency-doubled c-cut composite Nd:YVO_4 self-Raman laser. *Opt. Laser Technol.* **2021**, *133*, 106534. [CrossRef]
35. Li, Y.; Huang, X.; Mao, W.; Xu, J.; Duan, Y.; Zhu, H. Compact 589 nm yellow source generated by frequency-doubling of passively Q-switched Nd:YVO4 Raman laser. *Microw. Opt. Technol. Lett.* **2022**, *2022*, 1–5.
36. Chen, Y.F.; Hsieh, M.X.; Tu, Y.C.; Lee, C.C.; Yu, Y.T.; Tsou, C.H.; Liang, H.C. Pedagogically fast model to evaluate and optimize passively Q-switched Nd-doped solid-state lasers. *Opt. Lett.* **2021**, *46*, 1588–1591. [CrossRef]

37. Kalashnikov, V.L. Pulse shortening in the passive Q-switched lasers with intracavity stimulated Raman scattering. *Opt. Commun.* **2003**, *218*, 147–153. [CrossRef]
38. Chen, Y.F. Compact efficient self-frequency Raman conversion in diode–pumped passively Q-switched Nd:$GdVO_4$ laser. *Appl. Phys. B Lasers Opt.* **2004**, *78*, 685–687. [CrossRef]
39. Chen, Y.F. Efficient subnanosecond diode–pumped passively Q-switched Nd:YVO_4 self-stimulated Raman laser. *Opt. Lett.* **2004**, *29*, 1251–1253. [CrossRef]
40. Chen, Y.F.; Ku, M.L.; Tsai, L.Y.; Chen, Y.C. Diode-pumped passively Q-switched picosecond Nd:$Gd_xY_{1-x}VO_4$ self-stimulated Raman laser. *Opt. Lett.* **2004**, *29*, 2279–2281. [CrossRef]
41. Mochalov, I.V. Laser and nonlinear properties of the potassium gadolinium tungstate laser crystal KGd $(WO_4)_2$:Nd^{3+}-(KGW: Nd). *Opt. Eng.* **1997**, *36*, 1660–1669. [CrossRef]